Lawrence Berkeley National Laboratory
LBL Publications

Title
New insights into the low-temperature oxidation of 2-methylhexane

Permalink
https://escholarship.org/uc/item/90c8t2s9

Journal
Proceedings of the Combustion Institute, 36(1)

ISSN
1540-7489

Authors
Wang, Zhandong
Mohamed, Samah Y
Zhang, Lidong
et al.

Publication Date
2017

DOI
10.1016/j.proci.2016.06.085

Peer reviewed

New insights into the low-temperature oxidation of 2-methylhexane

Zhandong Wang [a,*], Samah Y. Mohamed [a], Lidong Zhang [b],
Kai Moshammer [c], Denisia M. Popolan-Vaida [d,e],
Vijai Shankar Bhavani Shankar [a], Arnas Lucassen [f], Lena Ruwe [g],
Nils Hansen [c], Philippe Dagaut [h], S. Mani Sarathy [a]

[a] *King Abdullah University of Science and Technology (KAUST), Clean Combustion Research Center (CCRC), Thuwal 23955-6900, Saudi Arabia*
[b] *National Synchrotron Radiation Laboratory, University of Science and Technology of China, Hefei, Anhui 230029, PR China*
[c] *Combustion Research Facility, Sandia National Laboratories, Livermore, CA 94551, USA*
[d] *Departments of Chemistry, University of California, Berkeley, CA 94720, USA*
[e] *Chemical Sciences Division, Lawrence Berkeley National Laboratory, Berkeley, CA 94720, USA*
[f] *Physikalisch-Technische Bundesanstalt, Bundesallee 100, D-38116 Braunschweig, Germany*
[g] *Department of Chemistry, Bielefeld University, D-33615 Bielefeld, Germany*
[h] *Centre National de la Recherche Scientifique (CNRS), INSIS, 1C, Avenue de la recherche scientifique, 45071 Orléans Cedex 2, France*

Abstract

In this work, we studied the low-temperature oxidation of a stoichiometric 2-methylhexane/O_2/Ar mixture in a jet-stirred reactor coupled with synchrotron vacuum ultraviolet photoionization molecular-beam mass spectrometry. The initial gas mixture was composed of 2% 2-methyhexane, 22% O_2 and 76% Ar and the pressure of the reactor was kept at 780 Torr. Low-temperature oxidation intermediates with two to five oxygen atoms were observed. The detection of $C_7H_{14}O_5$ and $C_7H_{12}O_4$ species suggests that a third O_2 addition process occurs in 2-methylhexane low-temperature oxidation. A detailed kinetic model was developed that describes the third O_2 addition and subsequent reactions leading to $C_7H_{14}O_5$ (keto-dihydroperoxide and dihydroperoxy cyclic ether) and $C_7H_{12}O_4$ (diketo-hydroperoxide and keto-hydroperoxy cyclic ether) species. The kinetics of the third O_2 addition reactions are discussed and model calculations were performed that reveal that third O_2 addition reactions promote 2-methylhexane auto-ignition at low temperatures.
© 2016 The Combustion Institute. Published by Elsevier Inc. All rights reserved.

Keywords: Auto-oxidation; Highly oxidized multifunctional molecules; Peroxides; Alternative isomerization; Synchrotron VUV photoionization mass spectrometry

* Corresponding author.
 E-mail address: zhandong.wang@kaust.edu.sa (Z. Wang).

1. Introduction

Detailed kinetic models for hydrocarbon fuels are important for improving combustion efficiency and reducing pollutant emission. Among real fuels (e.g., gasoline, diesel, and jet fuels), straight-chain (normal) and branched (iso) paraffins are common species, and thus selected as important components in surrogate fuels [1,2]. This study is concerned with the auto-oxidation of 2-methylhexane, which is an important component for surrogate fuels [1–3]. It is a continuation of the earlier work of Wang et al. [4] in which the oxidation of 2,5-dimethylhexane was studied. This work is of particular interest because detailed studies on heptane isomers have revealed that low-temperature auto-oxidation and auto-ignition are particularly affected by the number and location of methyl branches [5,6].

Kinetic models for oxidation of large hydrocarbons are typically developed using reaction classes and rate rules [7]. To simulate low-temperature auto-oxidation chemistry, the classical reaction scheme involving the O_2 addition on fuel radicals (R) and hydroperoxy alkyl radicals (QOOH) (note: $R=C_nH_{2n+1}$, $Q=C_nH_{2n}$) is commonly adopted [8]. Recently, Ranzi et al. [9] proposed three new reaction classes in the low-temperature auto-oxidation of n-alkanes, i.e., H-atom abstraction from keto-hydroperoxides to form dicarbonyl compounds, the Korcek decomposition mechanism of keto-hydroperoxides, and recombination/disproportionation reactions of peroxy radicals. Bugler et al. [10] and Zhang et al. [11] considered the alternative isomerization of hydroperoxy alkylperoxy radicals (OOQOOH) to dihydroperoxy alkyl radicals ($P(OOH)_2$, $P=C_nH_{2n-1}$) in the kinetic modeling of pentanes and n-hexane. In their reaction schemes, the $P(OOH)_2$ radicals decompose into hydroperoxy cyclic ethers and/or olefinic hydroperoxides. Wang et al. [4] detected highly oxidized multifunctional (HOM) molecules with five and four oxygen atoms during the auto-oxidation of 2,5-dimethylhexane in a jet-stirred reactor (JSR). The authors proposed a third O_2 addition reaction scheme to $P(OOH)_2$ radicals, which predicts additional radical chain branching intermediates. Wang and Sarathy [12] also studied the effect of the third O_2 addition reactions on the ignition of n-pentane and n-hexane. They found that the extended mechanism has only a slight effect on n-pentane ignition, but promotes n-hexane ignition at low temperatures.

Recently, Mohamed et al. [13] updated the thermodynamic data and the kinetic reaction mechanism for 2-methylhexane (2MHX) using updated group values and rate rules derived from quantum calculations and experiments. The model was compared against high- and low-temperature 2MHX ignition delay times measured in shock tube and rapid compression machine. The authors also in-vestigated the alternative isomerization pathways for OOQOOH radicals. This work studies the low-temperature oxidation chemistry of 2MHX in a JSR. Besides the well-known species governing auto-ignition, species with four and five oxygen atoms were detected, suggesting the existence of a third O_2 addition process also in 2MHX auto-oxidation. To simulate the experimental observation of the third O_2 addition process, the 2MHX chemical kinetic model from Mohamed et al. [13] was extended to include the third O_2 addition to $P(OOH)_2$ radicals and subsequent reactions of $OOP(OOH)_2$ radicals. This work describes the kinetics of 2-methylhexane low-temperature auto-oxidation with a focus on $C_7H_{14}O_3$ species (e.g., keto-hydroperoxdes (KHP) and hydroperoxy cyclic ethers (HPCE)), $C_7H_{14}O_2$ species (e.g., olefinic hydroperoxides (OHP)), $C_7H_{12}O_4$ species (e.g., diketo-hydroperoxides (DKHP) and keto-hydroperoxy cyclic ethers (KHPCE)), and $C_7H_{14}O_5$ species (e.g., keto-dihydroperoxides (KDHP) and dihydroperoxy cyclic ethers (DHPCE)). Finally, homogenous batch reactor simulations were performed to show that third O_2 addition reactions promote the low-temperature auto-ignition of 2MHX and predict better the ignition properties of 2MHX [13].

2. Experimental and computational methods

The experiment was performed at Terminal 3 of the Chemical Dynamics Beamline of the Advanced Light Source at the Lawrence Berkeley National Laboratory. The low-temperature oxidation of a stoichiometric 2MHX (2%)/O_2 (22%)/Ar (76%) mixture was investigated in a JSR ($V = 33.5\,cm^3$) coupled with a high-resolution time-of-flight molecular-beam mass spectrometer that relies on tunable synchrotron-generated vacuum ultraviolet (VUV) radiation for photoionization. The reactor was kept at a quasi-atmospheric pressure of 780 Torr and temperatures between 530 and 740 K. Gas flows were adjusted to achieve a residence time of 0.5 s. The temperature was measured by a K-type thermocouple located in the vicinity of the sampling position. The uncertainty in reactor temperature is estimated to be ±20 K [4]. The JSR product gases are analyzed by a custom-built reflectron time-of-flight system with a sensitivity of 1 ppm, a dynamic range of several orders of magnitude, and a mass resolution of $m/\Delta m \sim 2500$. The experimental method is similar to the work of Battin-Leclerc and Qi et al. [14–16]. Details of the experimental setup have been described by Moshammer et al. [17].

Theoretical computational chemistry is needed to interpret the complex mass spectra and to explore chemical structures based on observed ionization thresholds. To this end, adiabatic ionization energies (IE) were calculated from the composite

CBS-QB3 method [18] using Gaussian09 [19]. For each species, the structure has been optimized for minimum energy. However, the structure may not represent the global energy minimum. The uncertainty of the calculated IEs is estimated to be ± 0.05 eV [18], which does not include the uncertainty from excluding all conformeric structures. Calculated adiabatic ionization energies of conformeric structures can differ by as much as 0.5 eV [17], which basically precludes structural assignments.

3. Kinetic model development

Recently, Mohamed et al. [13] studied the ignition chemistry of 2MHX with a comprehensive chemical kinetic model. The low-temperature oxidation mechanism includes 20 classes of reactions in the classical reaction scheme [7], the alternative isomerization of OOQOOH to P(OOH)$_2$ [20,21], the subsequent decomposition of P(OOH)$_2$ (e.g., C–O β-scission), and their cyclization to HPCE and OH [10,11]. Only formation of P(OOH)$_2$ radicals derived from the OOQOOH via six-membered transition state (TS) ring were considered. This simplification is reasonable because six-membered TS ring isomerizations are favorable in most cases compared with other TS geometries. The thermodynamic data and rate rules were updated with new group values [22] and quantum-chemistry calculations [20,21,23–25], respectively.

In this work, the third O$_2$ addition to P(OOH)$_2$, and subsequent pathways of OOP(OOH)$_2$ were added to the 2MHX kinetic model of Mohamed et al. [13] following a similar methodology proposed by Wang et al. [4,12]. The subsequent pathways of OOP(OOH)$_2$ include the following three classes: (i) H-atom migrations of the C–H attached to the –OOH group and CO β-scission to KDHP + OH; (ii) intramolecular H-atom migrations of the C–H attached to the non –OOH group to form T(OOH)$_3$, which cyclizes to DHPCE + OH and/or C–O β-scission to olefinic dihydroperoxides (ODHP) + HO$_2$; and (iii) concerted eliminations of HO$_2$ to form ODHP. Alternative isomerization of OOP(OOH)$_2$ to T(OOH)$_3$ via six-membered TS rings were considered, while seven-membered TS ring isomerizations were considered when six-membered TS ring isomerizations are not available. H-atom abstractions from KDHP and DHPCE were included with subsequent decomposition to DKHP and KHPCE, respectively [4,12]. The decompositions of KDHP, DHPCE, ODHP, DKHP, and KHPCE were treated analogously to the decomposition of KHP (i.e., homolytic dissociation of –OOH). Scheme 1 presents the detailed reaction pathways of OOQOOH radicals, wherein alternative isomerizations and subsequent reactions are highlighted. The thermodynamic of new species were estimated using the THERM software [26] with new group values from Burke et al. [22].

Table 1 shows the rate rules utilized in the third O$_2$ addition reaction mechanism, which were derived by analogy to similar reactions of QOOH, OOQOOH, P(OOH)$_2$, and KHP from Mohamed et al. [13] to ensure self-consistency within the kinetic model. The detailed model of 2MHX is provided in the Supplemental Material (SM). The kinetic model was compared against the experimental JSR data using transient perfectly stirred reactor simulations in the CHEMKIN PRO software [27] with an end time of 20 s. This is an arbitrary number wherein the only important criteria is to run the simulation long enough so that species mole fractions cease to change with time.
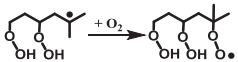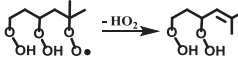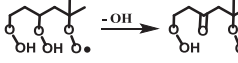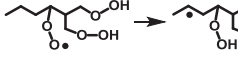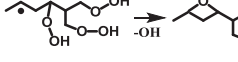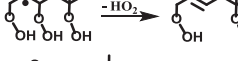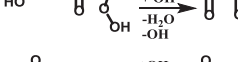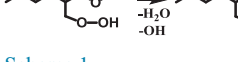
4. Results and discussion

Figure 1a shows the mass spectrum in the range of $m/z = 126$–180 taken at 10.5 eV and a reactor temperature of 560 K. The molecular formula for a specific m/z signal depends on kinetic analyses, following the methodology of Wang et al. [4]. According to the classical and extended reaction scheme [4], we identified m/z values at 130.10, 146.09, 160.07, and 178.08 as C$_7$H$_{14}$O$_2$, C$_7$H$_{14}$O$_3$, C$_7$H$_{12}$O$_4$, and C$_7$H$_{14}$O$_5$, respectively. The temperature distributions of the above species were measured, but mole fraction quantification was not feasible due to the lack of absolute photoionization cross sections for species at these m/z values. Thus only the temperature dependent mass spectrometer signals of these species are compared with the simulated profiles. Quantitative measurements of 2MHX were possible because its calibration factor was calculated based on the flow conditions at 530 K (assuming that no oxidation reactions occur at this temperature); its measured concentration is captured by the kinetic model indicating a good reproduction of global reactivity (Fig. 1b). In addition, the mass peaks corresponding to C$_7$H$_{13}$O$_2$ (m/z 129.10) and C$_7$H$_{13}$O$_3$ (m/z 145.09) were also observed, which may originate from the fragmentation of larger molecules such as C$_7$H$_{14}$O$_3$ and C$_7$H$_{14}$O$_5$ at 10.5 eV, respectively.

The present study focuses on tentatively assigning probable structures of several key intermediates based on measured photoionization efficiency (PIE) curves, calculated ionization energies, but mainly modeled concentration profiles. Here, we focus on the kinetics of KHP formation and new reaction pathways in our extended auto-oxidation scheme (i.e., the alternative isomerization of OOQOOH and third O$_2$ addition reaction scheme).

4.1. KHP formation from OOQOOH

The O$_2$ addition to QOOH radicals produces OOQOOH radicals, whose H-atom migration from

Table 1
Rate rules utilized for the third O_2 addition reaction mechanism.

Reactions	Reaction type	Analogous reaction	Refs.	Example
$O_2 + P(OOH)_2 = OOP(OOH)_2$	O_2 addition	$O_2 + QOOH = OOQOOH$	[21]	
$OOP(OOH)_2 = ODHP + HO_2$	Concerted elimination	$OOQOOH = OHP + HO_2$	[23]	
$OOP(OOH)_2 = KDHP + OH$	H-migration, β-scission	$OOQOOH = KHP + OH$	[20]	
$OOP(OOH)_2 = T(OOH)_3$	H-migration	$OOQOOH = P(OOH)_2$	[23]	
$T(OOH)_3 = DHPCE + OH$	Cyclization	$P(OOH)_2 = HPCE + OH$	[24]	
$T(OOH)_3 = ODHP + HO_2$	C-O β-scission	$P(OOH)_2 = OHP + HO_2$	[25]	
$KDHP + OH = H_2O + OH + DKHP$	H-abstraction, β-scission	$KHP + OH = H_2O + OH + DKET$	[9]	
$DHPCE + OH = H_2O + OH + KHPCE$	H-abstraction, β-scission	$KHP + OH = H_2O + OH + DKET$	[9]	
ODHP, KDHP, DHPCE, DKHP, and KHPCE decomposition	-OOH dissociation	$KHP = products$	[11]	Scheme 1
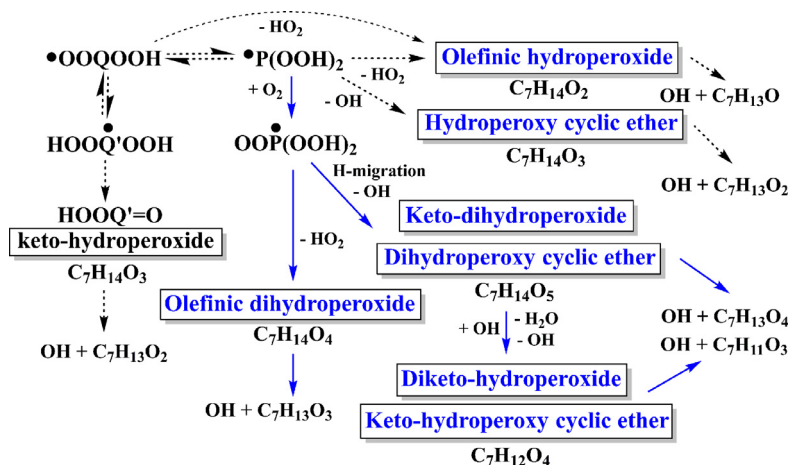
Scheme 1. Extended reaction scheme of OOQOOH radical [4,12]. The pathways included in 2MHX kinetic model [13] are annotated with dashed arrows; the extended third O_2 addition pathways studied in this work are annotated with blue solid lines.
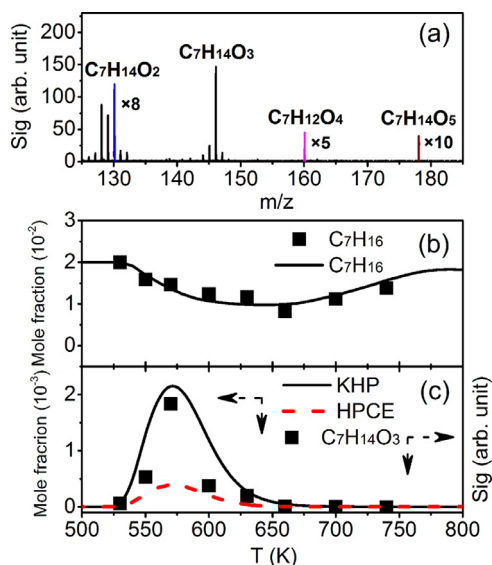

Fig. 1. (a) Mass spectrum from 2MHX oxidation at 560 K and photon energy of 10.5 eV. The peaks labeled with a molecular formula are discussed in the text; (b) Temperature dependent profiles for the measured (symbols) and simulated (lines) mole fraction of 2MHX; and (c) the signal of $C_7H_{14}O_3$ (symbols, right axis) and simulated mole fraction of KHP and HPCE (lines, left axis). (For interpretation of the references to color in this figure, the reader is referred to the web version of this article).

Fig. 2. Energy scan of $C_7H_{14}O_3$ in 2MHX low-temperature oxidation at 560 K. The signals annotated with red and circle are multiplied by a factor of 10 to denote the onset. (For interpretation of the references to color in this figure legend, the reader is referred to the web version of this article).

the C–H alpha to the hydroperoxy (–OOH) forms HOOQ′OOH radicals. The HOOQ′OOH radicals are α-hydroperoxyalkylhydroperoxy radicals and can decompose to KHP and OH radicals (Scheme 1). The former is the main chain branch-ing species, which further decomposes to generate more OH radicals.
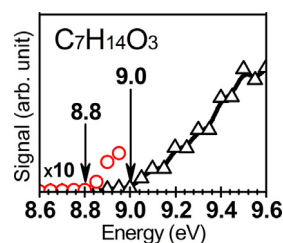
This study observed a peak with m/z 146.09, which corresponds to $C_7H_{14}O_3$ (KHP). As will be discussed later, the $C_7H_{14}O_3$ profile may also in-clude HPCE. The simulated KHP profiles repro-duce the measured temperature-dependent profile of $C_7H_{14}O_3$ in Fig. 1c. Figure 2 shows the energy scan for m/z 146.09, and clear onsets appear at 8.8 and 9.0 eV. The calculated IEs of 24 potential KHP isomers were found to range from 8.83 to 9.46 eV when neglecting effects of conformeric structures. (see Table S1 in the SM). The calculated IEs of more than 10 species are near the observed thresh-olds at 8.8 and 9.0 eV, thus making a definitive iso-meric assignment impossible.

The modeling calculations predict that the six most abundant isomers are 2-methyl-2-hydroperoxy-hexan-4-one (KHP-1 in Table S1, mole fraction: 7.9×10^{-4}), 2-methyl-5-hydrope-

roxy-hexan-3-one (KHP-2, mole fraction: 7.2×10^{-4}), 2-methyl-2-hydroperoxy-hexan-5-one (KHP-3, mole fraction: 4.1×10^{-4}), 2-methyl-3-hydroperoxy-hexanal (KHP-4, mole fraction: 1.4×10^{-4}), 2-methyl-3-hydroperoxy-hexan-5-one (KHP-5, mole fraction: 4.6×10^{-5}), and 5-methyl-5-hydroperoxy-hexanal (KHP-6, mole fraction: 3.0×10^{-5}). Except for KHP-3 and KHP-6, the hydroperoxy and carbonyl functional groups of the other four KHPs (e.g., KHP-1, KHP-2, KHP-4, and KHP-5) is separated by one carbon atom, indicating that ROO radicals mainly isomerize via six-membered TS rings. The formation of KHP-3 and KHP-6 indicates that the seven-membered and eight-membered TS ring isomerizations are competitive with six-membered TS ring isomerizations, especially when a tertiary C–H bond is involved [23].

4.2. Alternative isomerization of OOQOOH to P(OOH)₂

Recently, Bugler et al. [10] and Zhang et al. [11] developed detailed kinetic models for pentanes and n-hexane to study their ignition chemistry. The authors proposed the alternative isomerization of OOQOOH to P(OOH)$_2$, which further cyclize to HPCE and OH and/or decompose to OHP and HO$_2$ (Scheme 1). The P(OOH)$_2$ was selected to denote the alternative isomerization products, which is distinct from the HOOQ′OOH produced from the classical scheme. It should be noted that P(OOH)$_2$ has the same molecular formula as HOOQ′OOH, but the radical positions are different. In this work, we detected signal at *m/z* values of 130.10 and 146.09, which correspond to OHP ($C_7H_{14}O_2$) and HPCE or KHP ($C_7H_{14}O_3$), respectively. The 2MHX model by Mohamed et al. [13] already includes alternative isomerization of OOQOOH radicals and the subsequent decomposition of P(OOH)$_2$ radicals.

Figure 3a and b presents the PIE spectra and temperature-dependent profile of $C_7H_{14}O_2$. The simulated temperature distribution of OHP agrees with the measurement at lower temperature, but decays faster after 600 K. The reaction mechanisms suggests that $C_7H_{14}O_2$ are likely to be olefinic hydroperoxides, but other isomers such as with alcohol and carbonyl groups may also exist. The rise in signal above 600 K might be due to the existence of other isomers and/or due to the scatter of the signal. The concerted elimination of HO$_2$ from OOQOOH also forms OHPs. However, the JSR simulations show that these pathways are not dominant at the temperature range studied here. Table S2 shows the calculated IEs for the two most abundant OHPs from JSR simulations, i.e., 8.87 eV (OHP-1 in Table S2, 2-methyl-2-hydroperoxy-hex-4-ene, mole fraction: 4.7×10^{-5}) and 8.41 eV (OHP-2, 2-methyl-5-hydroperoxy-hex-2-ene, mole fraction: 3.2×10^{-5}),
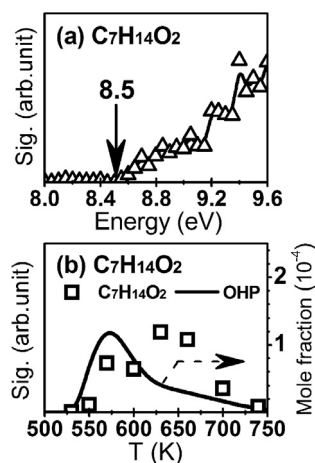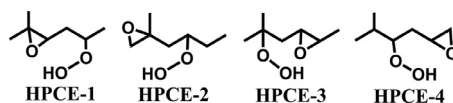

Fig. 3. (a) Energy scan of $C_7H_{14}O_2$ from 2MHX low-temperature oxidation at 560 K. (b) Temperature dependent profiles for the measured signal (symbol) and simulated mole fraction (line, right axis) of $C_7H_{14}O_2$.

Scheme 2. The structures of the most abundant HPCEs.

respectively. Figure 3a shows a measured IE onset of 8.5 eV, which is close to that of OHP-2, but ~0.4 eV lower than that of OHP-1. Although the mole fraction of OHP-1 is higher than that of OHP-2, its IE onset of 8.87 eV is not evident in Fig. 3a.

The cyclization of P(OOH)$_2$ radicals forms HPCE species, which have the same formula as KHP. The separation of HPCE from KHP is not feasible in the experiment. In this study, we tried to elucidate the HPCE structures only from the JSR simulations. The red dashed line in Fig 1c is the sum of the predicted HPCE mole fractions. In total the peak value is ~17% that of KHP. The modeling results show that HPCEs are mainly composed of HPCE-1 (mole fraction: 1.9×10^{-4}), HPCE-2 (mole fraction: 1.0×10^{-4}), HPCE-3 (mole fraction: 6.6×10^{-5}), and HPCE-4 (mole fraction: 2.0×10^{-5}). These HPCEs in Scheme 2 are three-membered-ring cyclic ethers, having an –OOH attached to the secondary or tertiary carbon site and having a carbon atom separating the two functional groups. This analysis reveals that HPCEs are produced from the β,γ-P(OOH)$_2$ radical, which requires that ROO isomerizes to QOOH via seven-membered TS rings, and OOQOOH isomerizes to P(OOH)$_2$ via six-membered TS rings (the position of a carbon bonded to an –OOH group in a P(OOH)$_2$ radical is designated by α, β, γ, δ, ε, re-
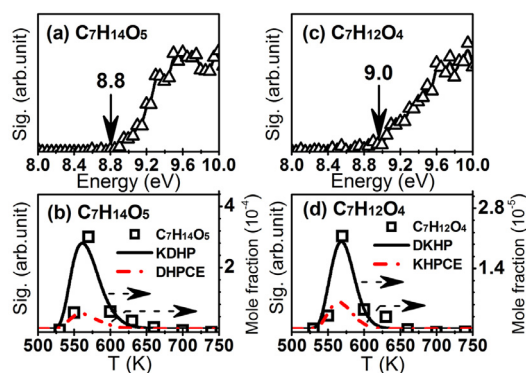
Fig. 4. Energy (upper) and temperature (lower) scans of (a, b) $C_7H_{14}O_5$ and (c, d) $C_7H_{12}O_4$ in 2MHX low-temperature oxidation at 560 K and 9.5 eV, respectively. The symbols are measured signal and lines (right axis) are the simulated mole fractions in (b) and (d).

spectively; α position is the carbon site with the radical).

4.3. Third O_2 addition to $P(OOH)_2$

Two high-molecular-weight species with m/z values 160.07 ($C_7H_{12}O_4$) and 178.08 ($C_7H_{14}O_5$) were detected in this work. The observation of $C_7H_{14}O_5$ species indicates the presence of further O_2 addition process, e.g., $O_2 + P(OOH)_2$, during 2MHX low-temperature oxidation. The third O_2 addition process was also observed during 2,5-dimethylhexane low-temperature oxidation by Wang et al. [4]. $C_7H_{14}O_5$ species have two probable structures, i.e., KDHP and DHPCE (Scheme 1 and Table 1). For OOP(OOH)$_2$ radicals, intramolecular H-atom migrations from the C–H alpha to the –OOH group and subsequent C-O β-scission produce KDHP + OH, while intramolecular H-atom migrations from the C–H not attached to the –OOH group form T(OOH)$_3$ that further cyclize to DHPCE + OH.

Figure 4a and b presents the energy and temperature scans for $C_7H_{14}O_5$ species. The predicted mole fractions of 43 probable KDHPs and 9 probable DHPCEs capture the temperature dependent distribution of $C_7H_{14}O_5$ species. We calculated the IEs of 10 KDHPs having mole fractions higher than 1 ppm (i.e., the detection limit of experiment), and their IEs in Table S3 range from 8.47 up to 9.45 eV.

Scheme 3 presents the reaction pathways for the seven most abundant KDHP isomers from simulations, i.e., KDHP-1 (mole fraction: 6.9×10^{-5}), KDHP-2 (mole fraction: 6.4×10^{-5}), KDHP-3 (mole fraction: 4.2×10^{-5}), KDHP-4 (mole fraction: 4.0×10^{-5}), KDHP-5 (mole fraction: 2.7×10^{-5}), KDHP-6 (mole fraction: 2.5×10^{-5}), and KDHP-7 (mole fraction: 1.3×10^{-5}). The formation of these KDHPs competes with the cyclization of P(OOH)$_2$ to HPCE, such as HPCE-1,

HPCE-2, and HPCE-3 in Scheme 2, and produce additional OH radicals [12]. The kinetics of KDHP formation based on the simulations are analyzed. First, the OOQOOH radicals produced from isomerization of ROO radicals via seven-membered (e.g., reaction a, f and g) and eight-membered TS rings (e.g., reaction b and c) can easily undergo alternative isomerizations via six-membered TS rings; these reactions compete with the isomerization and formation of KHP via seven- and/or eight- membered TS rings. In addition, OOQOOH radicals from the primary fuel radical favor alternative isomerizations [4] (e.g., reactions a-e), which subsequently produce more KDHP. The presence of a tertiary carbon site also facilitates the third O_2 addition process because its lower C-H bond strength facilitates alternative isomerizations (e.g., reaction a, b, d, and f). Finally, OOQOOH radicals from the tertiary fuel radical cannot produce KHP, but can undergo alternative isomerization and third O_2 addition, and finally form KDHP. Compared with the classical reaction scheme, reaction g shows that third O_2 addition reactions divert the carbon flux to more reactive KDHP species.

The predicted mole fraction of DHPCEs in Fig. 4b is ~20% that of KDHPs because the further alternative isomerizations of OOP(OOH)$_2$ radicals to T(OOH)$_3$ radicals are less favorable than their isomerization and decomposition to KDHPs. Scheme 4 shows the reaction pathways for DHPCE-1, an important isomer for DHPCE.

Figure 4c and d shows the energy and temperature scans of $C_7H_{12}O_4$ species. The potential structures of $C_7H_{12}O_4$ species are DKHP and KHPCE (Scheme 1 and Table 1), which are produced from the H-atom abstraction of $C_7H_{14}O_5$ species, KDHP and DHPCE, respectively. The simulated mole fraction profiles of DKHP and KHPCE capture the temperature-dependent distribution of $C_7H_{12}O_4$ species. The distribution of DKHP and KHPCE structures is related to the KDHP and
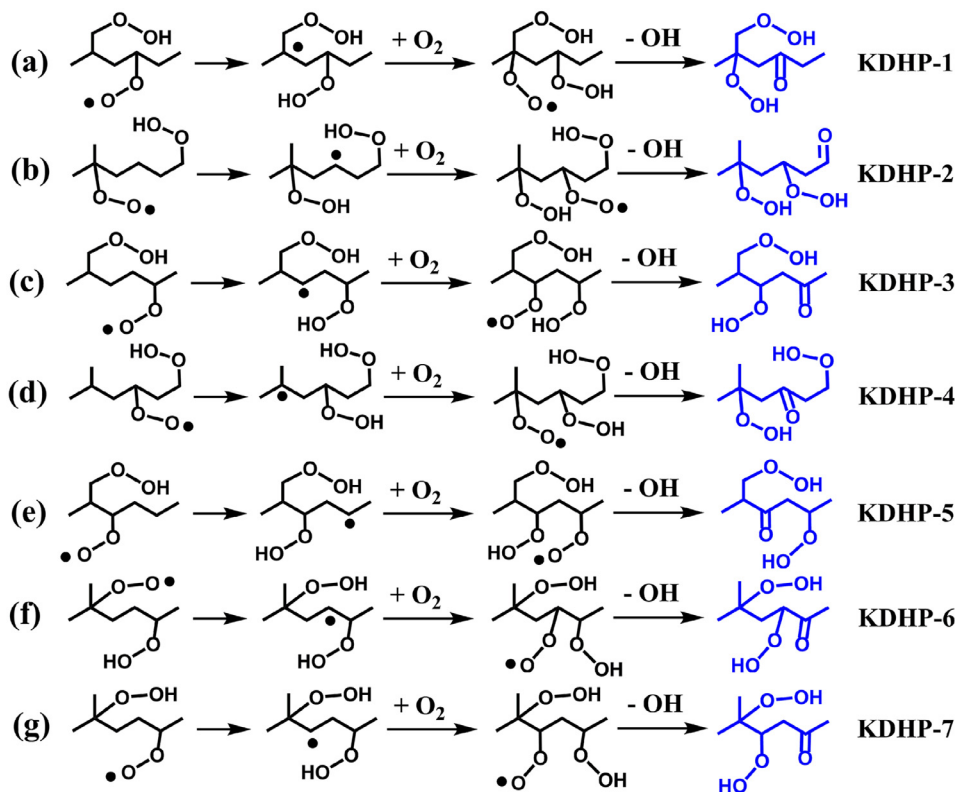
Scheme 3. Selected reactions for OOQOOH alternative isomerization, third O_2 addition, and decomposition to KDHP.
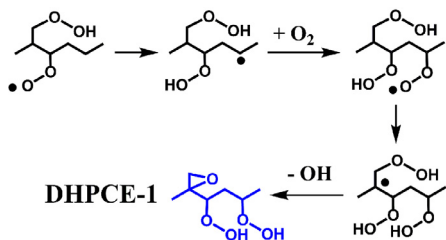
Scheme 4. Reaction pathways for DHPCE-1 formation.

DHPCE structures from which they are derived. This study calculated the IEs of 5 DKHPs having mole fractions higher than 1 ppm, which range from 9.11 up to 9.54 eV (Table S4).

4.4. 2MHX ignition simulations

Recently, Wang and Sarathy [12] studied the effect of third O_2 addition reactions on n-pentane and n-hexane low-temperature auto-ignition. The authors showed that the third O_2 addition reactions only slightly promotes n-pentane ignition, but significantly advances n-hexane ignition. In

this work we studied the effects of the third O_2 addition on the ignition of a lean 2MHX/air mixture at 20 and 40 bar [13]. The ignition delay time was calculated in a closed homogenous batch reactor with constant volume profiles, using the CHEMKIN-Pro software [27].

Figure 5a shows that including the third O_2 addition scheme reduces ignition delay time by a factor of two at 620 K (20 and 40 bar). The promotion is gradually diminished as temperature increases; for example, the ignition delay time is only 10% faster at 750 K. As temperature increases, the third O_2 addition reaction is inhibited by chemical equilibrium. In general, considering the third O_2 addition and subsequent reactions improves the prediction of ignition delay time under the studied conditions. To elucidate the chemical effect of third O_2 addition reactions, we compared the time-dependent distribution of key intermediates during ignition, such as OH, KHP, HPCE, $C_7H_{14}O_5$, and $C_7H_{12}O_4$ species at 620 K and 20 bar. The results in Fig. 5b–f show that the third O_2 addition reactions cause OH, KHP, and HPCE to be produced at earlier time scales. The third O_2 addition reactions slightly decrease the peak mole fraction of KHP and significantly decrease that of HPCE, thereby
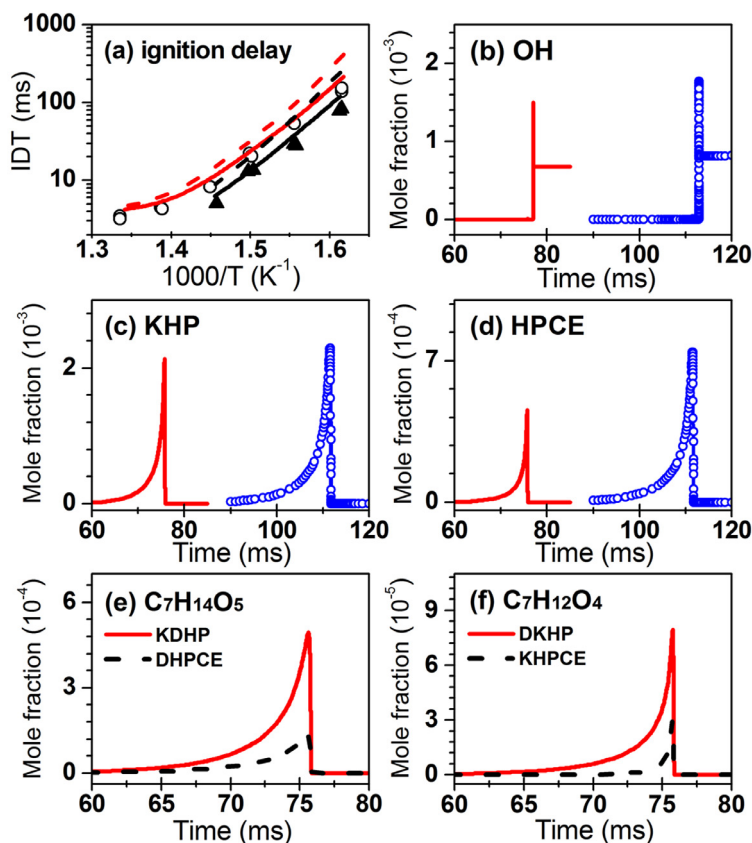
Fig. 5. (a) Ignition delay times for 2MHX/air mixtures at $\varphi = 0.5$, 20 and 40 bar. The open circle, red dash line, and red solid line are ignition delay time by experiment, simulation without third O_2 addition reactions, and simulation with third O_2 addition reactions at 20 bar, respectively; The solid triangle, black dash line, and black solid line are ignition delay time by experiment, simulation without third O_2 addition reactions, and simulation with third O_2 addition reactions at 40 bar, respectively. (b)–(f) Time-dependent distribution of OH, KHP, HPCE, $C_7H_{14}O_5$, and $C_7H_{12}O_4$ at 620 K and 20 bar. Open symbols and blue lines: simulation without third O_2 addition reactions [13]; lines: simulation with third O_2 addition reactions. (For interpretation of the references to color in this figure legend, the reader is referred to the web version of this article).

diverting the carbon flux to $C_7H_{14}O_5$ (KDHP and DHPCE) and $C_7H_{12}O_4$ (DKHP and KHPCE) species.

The initial accumulation of chain branching intermediates and their subsequent decomposition to release OH radicals drives the auto-ignition process. $C_7H_{14}O_3$ species (KHP and HPCE) are the chain branching species in simulations without the third O_2 addition reactions. When the third O_2 addition reactions are considered, both $C_7H_{14}O_3$ (KHP and HPCE) and $C_7H_{14}O_5$ (KDHP and DHPCE) become the chain branching intermediates. Although the concentration of $C_7H_{14}O_5$ species is only 30% of that of the $C_7H_{14}O_3$ species, the barrierless third O_2 addition reactions result in the formation of chain-branching precursors at lower temperatures (i.e., earlier reaction times) [12]. Thus, the formation and destruction of $C_7H_{14}O_5$ species

accelerates the accumulation of OH radicals and advances auto-ignition.

5. Conclusions

In this work, we studied the low-temperature oxidation chemistry of 2MHX through JSR oxidation experiment and kinetic modeling. Several key intermediates controlling the auto-ignition process, especially OHP, $C_7H_{14}O_3$, $C_7H_{14}O_5$, and $C_7H_{12}O_4$ species, were observed. The mechanisms leading to their formation were elucidated with chemical kinetic simulations. The simulations reveal that the primary and tertiary carbon sites of 2MHX facilitate the extended low-temperature auto-oxidation scheme. The extended reaction mechanism, promotes low-temperature auto-ignition of 2MHX

due to the barrierless third O_2 addition reactions, accompanied by the formation and destruction of $C_7H_{14}O_5$ species (KDHP and DHPCE) to form additional OH radicals.

Supplementary materials

The structures and calculated ionization energies in Table S1–S4 for $C_7H_{14}O_3$, $C_7H_{14}O_2$, $C_7H_{14}O_5$, and $C_7H_{12}O_4$ species; 2MHX kinetic model including the third O_2 addition and subsequent reactions.

Supplementary material associated with this article can be found, in the online version, at doi:10.1016/j.proci.2016.06.085.

References

[1] S.M. Sarathy, G. Kukkadapu, M. Mehl, et al., *Proc. Combust. Inst.* 35 (2015) 249–257.
[2] A. Ahmed, G. Goteng, V.S.B. Shankar, K. Al-Qurashi, W.L. Roberts, S.M. Sarathy, *Fuel* 143 (2015) 290–300.
[3] S.M. Sarathy, G. Kukkadapu, M. Mehl, et al., *Combust. Flame* 169 (2016) 171–193.
[4] Z.D. Wang, L. Zhang, K. Moshammer, et al., *Combust. Flame* 164 (2016) 386–396.
[5] C.K. Westbrook, W.J. Pitz, H.C. Curran, J. Boercker, E. Kunrath, *Int. J. Chem. Kinet.* 33 (2001) 868–877.
[6] E.J. Silke, H.J. Curran, J.M. Simmie, *Proc. Combust. Inst.* 30 (2005) 2639–2647.
[7] S.M. Sarathy, C.K. Westbrook, M. Mehl, et al., *Combust. Flame* 158 (2011) 2338–2357.
[8] F. Battin-Leclerc, *Prog. Energy Combust. Sci.* 34 (2008) 440–498.
[9] E. Ranzi, C. Cavallotti, A. Cuoci, A. Frassoldati, M. Pelucchi, T. Faravelli, *Combust. Flame* 162 (2015) 1679–1691.
[10] J. Bugler, K.P. Somers, E.J. Silke, H.J. Curran, *J. Phys. Chem. A* 119 (2015) 7510–7527.
[11] K. Zhang, C. Banyon, C. Togbé, P. Dagaut, J. Bugler, H.J. Curran, *Combust. Flame* 162 (2015) 4194–4207.
[12] Z.D. Wang, S.M. Sarathy, *Combust. Flame* 165 (2016) 364–372.
[13] S.Y. Mohamed, L. Cai, F. Khaled, et al., *J. Phys. Chem. A* 120 (2016) 2201–2217.
[14] F. Battin-Leclerc, O. Herbinet, P.-A. Glaude, et al., *Angew. Chem. Int. Ed.* 49 (2010) 3169–3172.
[15] F. Battin-Leclerc, O. Herbinet, P.-A. Glaude, et al., *Proc. Combust. Inst.* 33 (2011) 325–331.
[16] F. Qi, *Proc. Combust. Inst.* 34 (2013) 33–63.
[17] K. Moshammer, A.W. Jasper, D.M. Popolan-Vaida, et al., *J. Phys. Chem. A* 119 (2015) 7361–7374.
[18] J.A. Montgomery, M.J. Frisch, J.W. Ochterski, G.A. Petersson, *J. Chem. Phys.* 110 (1999) 2822–2827.
[19] M.J. Frisch et al. Gaussian 09, Gaussian, Inc., Wallingford CT, (2009).
[20] S. Sharma, S. Raman, W.H. Green, *J. Phys. Chem. A* 114 (2010) 5689–5701.
[21] A. Miyoshi, *J. Phys. Chem. A* 115 (2011) 3301–3325.
[22] S.M. Burke, J.M. Simmie, H.J. Curran, *J. Phys. Chem. Ref. Data* 44 (2015) 013101.
[23] S.M. Villano, L.K. Huynh, H.-H. Carstensen, A.M. Dean, *J. Phys. Chem. A* 115 (2011) 13425–13442.
[24] S.M. Villano, L.K. Huynh, H.-H. Carstensen, A.M. Dean, *J. Phys. Chem. A* 116 (2012) 5068–5089.
[25] S.M. Villano, H.-H. Carstensen, A.M. Dean, *J. Phys. Chem. A* 117 (2013) 6458–6473.
[26] E.R. Ritter, J.W. Bozzelli, *Int. J. Chem. Kinet.* 23 (1991) 767–778.
[27] CHEMKIN-PRO 15112, Reaction Design: San Diego, (2012).